Optics Letters

Polarization-controlled hybrid laser with high-power, narrow-linewidth, and widely tunable NIR emission

Donglin Cheng,[1] Xuechen Cao,[1] Yanan Chen,[1] Yan Wang,[1] Xiaojun Jia,[1,2,4] and Huadong Lu[1,2,3,*]

[1]State Key Laboratory of Quantum Optics Technologies and Devices, Institute of Opto-Electronics, Shanxi University, Taiyuan 030006, China
[2]Collaborative Innovation Center of Extreme Optics, Shanxi University, Taiyuan 030006, China
[3]National Key Laboratory of Particle Transport and Separation Technology, Tianjin, China
[4]jiaxj@sxu.edu.cn
*lu_sxu@163.com

Received 18 February 2026; revised 23 March 2026; accepted 28 March 2026; posted 30 March 2026; published 14 April 2026

We demonstrate a compact hybrid laser cavity that enables dynamic impedance matching via polarization control, which achieves high-power, narrow-linewidth, and widely tunable near-infrared (NIR) laser emission. By rotating the nonlinear crystal to distribute the parametric gain between orthogonal polarizations, low-loss intracavity oscillation for the *p*-polarized field and high-efficiency output for the *s*-polarized signal are simultaneously achieved, which resolves the inherent conflict in output coupling requirements between the Ti:sapphire population inversion and the optical parametric oscillator (OPO). At the same time, this mechanism also introduces a nonreciprocal gain to inherently suppress the backward propagation and realize the unidirectional laser operation without an optical isolator. The laser produces ns pulses tunable from 963.26 nm to 1003.32 nm. At 992 nm, it achieves a narrow linewidth of 169.5 MHz and an output power of 9.2 W under 52 W of total 532 nm pump power, which corresponds to an optical-to-optical conversion efficiency of 17.7%. This compact design operates without active mode control or external seed injection and offers a novel, to the best of our knowledge, pathway to high-performance tunable near-infrared lasers. © 2026 Optica Publishing Group. All rights, including for text and data mining (TDM), Artificial Intelligence (AI) training, and similar technologies, are reserved.

https://doi.org/10.1364/OL.593202

Tunable near-infrared (NIR) laser sources with high power and narrow linewidth are indispensable in cutting-edge fields including high-resolution spectroscopy [1], quantum information science [2], cold atom physics [3], and quantum state manipulation [4]. Furthermore, it is easy to extend the laser wavelength to the mid-infrared [5] and the ultraviolet [6,7] wavelength ranges through the nonlinear frequency conversion, which satisfies the requirements of broader applications such as imaging, sensing, and materials processing.

The Ti:sapphire crystal is the most popular candidate for generating tunable near-infrared (NIR) light because its fluorescence spectrum covers the broad range from 700 nm to 1000 nm. Gain-switching is often employed to produce high-energy ns pulses due to its short upper-level lifetime (3.2 μs) [8]. However, it is difficult to obtain the high-power operation because of its severe thermal effects [9–12]. Meanwhile, the optical parametric oscillator (OPO) based on nonlinear frequency conversion can generate high-power NIR light because it inherently avoids the thermal load associated with non-radiative relaxation processes in conventional laser gain media. However, the linewidth of a free-running OPO is typically as broad as several nanometers [13]. Consequently, we have to employ complex seed-injection and active phase-locking systems to narrow its linewidth, which adds substantial complexity and cost [14]. In 2025, our group developed a novel approach to overcome this challenge by integrating both the Ti:sapphire gain medium and the optical parametric process within a single resonator to directly generate a high-performance laser [15]. This scheme eliminated the requirement for complex external seed injection and achieved a maximum output power of 7.75 W at 830 nm with a narrow spectral width of 400.93 MHz. However, the requisite low-output coupling (13%) for the low-gain Ti:sapphire medium forced the OPO into an overcoupled state. This severely limited signal extraction, which caused most of the energy to dissipate inside the cavity and resulted in the low efficiency.

In response to these challenges, we propose a hybrid-gain resonator scheme based on the polarization control to significantly enhance the conversion efficiency. In this Letter, by adjusting the effective parametric gain via polarization, our approach simultaneously ensures a high-Q cavity for the Ti:sapphire laser and efficient extraction of the parametric signal, which achieves dynamic impedance matching between the two gain media. Furthermore, the parametric process introduces a non-reciprocal gain that inherently suppresses the backward-propagating mode, so that it enables stable unidirectional operation without an optical isolator.

Figure 1 depicts a compact polarization-controlled ring resonator which incorporates both a Ti:sapphire crystal and a non-critical phase-matched (NCPM) LBO crystal as the laser gain medium and the nonlinear OPO medium, respectively. When one pump laser (Pump1) is injected into the resonator to pump the Ti:sapphire crystal, a *p*-polarized laser beam is generated and

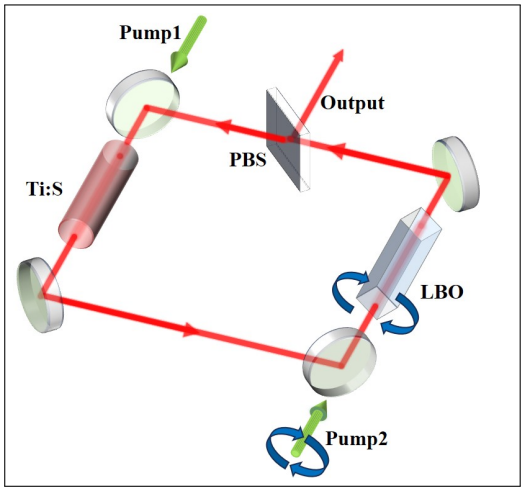


Fig. 1. Schematic of the hybrid cavity configurations.

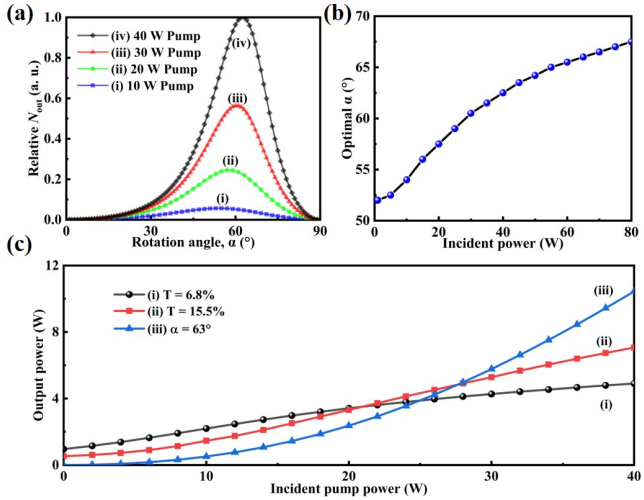


Fig. 2. Theoretical simulation of the hybrid cavity performance. (a) Calculated output photon number versus the LBO crystal rotation angle α at different incident pump powers. (b) Optimal angle and equivalent transmittance versus the pump power. (c) Output power scaling under three configurations: (i) fixed output coupler (6.8%), (ii) fixed output coupler (15.5%), and (iii) polarization control ($\alpha = 63^\circ$).

acts as the seed beam. Subsequently, when the other pump beam whose polarization keeps parallel to the z-axis of the LBO crystal (to satisfy type-I phase matching) is also injected to pump the LBO crystal, the generated seed beam from the Ti:sapphire crystal is then amplified through the optical parametric oscillation. Specifically, with the rotation of the LBO crystal, the amplified laser will be separated into the p-polarized and s-polarized laser beams. The p-polarized component continues to oscillate inside the cavity, while the s-polarized component is reflected out by the polarizing beam splitter (PBS). In other words, it is very easy to control the intracavity and output power of the designed laser. The dynamic characteristics of this hybrid gain cavity can be analyzed using a theoretical model which combines the laser rate equations with the parametric amplification process.

The coupled rate equations governing the evolution of the inversion population density (N) and the intracavity photon density (Φ) are:

$$\frac{dN}{dt} = W_s(t) - \sigma \frac{c}{n_s} N\Phi - \frac{N}{\tau_t}, \tag{1}$$

$$\frac{d\Phi}{dt} = G_{OPO}\Phi + \frac{V_s}{V_R}\sigma \frac{c}{n_s} N\Phi - \frac{\Phi}{\tau_R}, \tag{2}$$

where $W_s(t)$ is the pump rate density from Pump1, σ is the stimulated emission cross section, c is the speed of light in vacuum, n_s is the refractive index of the gain medium, τ_t and τ_R are the upper-level lifetime and photon lifetime respectively, V_s/V_R is the ratio of the gain medium mode volume to the resonator mode volume. The initial optical field is defined as a purely p-polarized wave within the laser's s/p coordinate system. When the laser enters the LBO crystal, it is transformed into the crystal's o/e coordinate system. The laser then experiences optical parametric gain within the LBO crystal, where only the o-ray component is amplified while the e-ray remains unchanged. Consequently, the net OPO gain G_{OPO} is derived as a function of the angle α between the intracavity laser polarization and the LBO crystallographic xOy plane:

$$G_{OPO} = \frac{1}{T_c} \ln\left[\left(G_E \cos^2\alpha + \sin^2\alpha\right)^2\right]. \tag{3}$$

Since the cavity round-trip time T_c (~0.65 ns) is much shorter than the pump pulse width (20 ns), the key term G_E is the single-pass field gain factor for the o-ray and can be calculated as follows [16]:

$$G_E = \sqrt{1 + \frac{\omega_s I_p}{\omega_p I_s}\sin^2\Gamma}, \tag{4}$$

where $\Gamma = \sqrt{\kappa_p \kappa_i |E_s \cos\alpha|} L$ represents the nonlinear phase shift accumulated along the LBO length L; $\kappa_p = \omega_p d_{eff}/(n_p c)$ and $\kappa_i = \omega_i d_{eff}/(n_i c)$ are the nonlinear coupling coefficients for the pump and idler waves respectively; E_s is the intracavity amplitude of the signal electric field and related to the intracavity photon density Φ; d_{eff} is the effective nonlinear coefficient of the LBO crystal and n_j (j = p,i,s) are the refractive indices of the crystal for the respective waves.

According to the derived rate equations, the optimal rotation angle α of the LBO crystal with the increase in its incident pump power is firstly calculated, where the power of Pump1 is fixed at 12 W. This value corresponds to the actual operating power used in the subsequent experiment to generate a stable Ti:sapphire seed laser, which ensures a direct comparison between the theoretical model and the experimental results. As shown in Fig. 2(a), the optimal angle increases from 55° at 10 W to 58°, 60°, and 63° at 20 W, 30 W, and 40 W, respectively. Figure 2(b) further illustrates the trend of the optimal rotation angle of the LBO crystal with the increase of the incident pump power. It is seen that the optimal rotation angle of LBO crystal increases with the increase in the incident pump power. However, this trend variation will gradually slow down when the incident pump power is further increased. The simulated output power of the hybrid cavity versus Pump2 power is shown in Fig. 2(c) for three configurations. Curve (i) represents a fixed output-coupler transmission of 6.8% ($\alpha = 0^\circ$, optimal for Ti:sapphire-only operation), where the output power rises slowly from 1.05 W to 4.2 W, as the incident power of Pump2 reaches 40 W with a

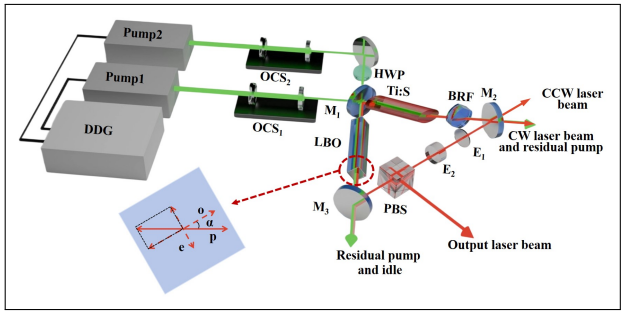


Fig. 3. Schematic diagram of the experimental setup for the polarization-controlled hybrid gain cavity. BF, birefringent filter; DDG, digital delay generator; Etalon, etalon; HWP, half-wave plate; M_1, M_2, M_3, cavity mirrors; LBO, nonlinear crystal (rotatable about the beam propagation axis by angle α); OCS_1, OCS_2: optical coupling systems; PBS, polarizing beam splitter (output coupler); Ti:S: titanium-sapphire crystal; Pump1 pumps Ti:S, Pump2 pumps LBO.

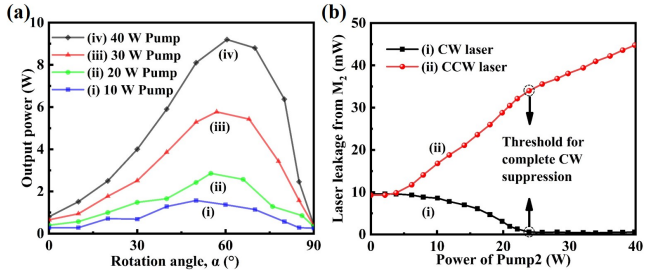


Fig. 4. (a) Measured output power versus LBO crystal rotation angle α for different pump powers. (b) The measured forward (CCW, curve (ii)) and backward (CW, curve (i)) optical power leaking from M_2 versus the Pump2 power.

low slope efficiency. Curve (ii) uses a higher fixed transmission of 15.5% (also $\alpha = 0°$, a compromise for simultaneous Ti:sapphire and OPO operation). Under this configuration, the output power increases more notably and reaches 7.2 W at a maximum pump power of 40 W. In contrast, curve (iii) corresponds to the polarization-controlled configuration, where the LBO crystal is rotated to the optimal angle ($\alpha = 63°$ at 40 W of Pump2). In this case, the Ti:sapphire laser remains confined inside the cavity and is not directly extracted, which initially results in lower output at low Pump2 power levels. As the pump power rises, the nonlinear gain is efficiently activated without saturation. As a result, the output overtakes Curve (i) at a Pump2 power of 25 W and surpasses Curve (ii) at 28 W, and ultimately reaches the highest predicted output of 10.4 W at a pump power of 40 W. These results confirm that a fixed output-coupler transmission cannot satisfy the differing gain needs of both media simultaneously, whereas dynamically adjusting the crystal orientation offers an effective way to suppress the saturation and enable high-power operation in a hybrid resonator.

To validate the theoretical model, we constructed a three-mirror ring resonator with a geometric length of 195 mm (Fig. 3), which effectively shortened the cavity length and reduced the intracavity loss. All cavity mirrors (M_1, M_2, M_3) were planar and coated with high transmission (HT) films at 532 nm and 1100–1200 nm, and high reflection (HR) films at 920–1000 nm. The intracavity gain medium was a $\Phi 4 \times 20$ mm titanium-sapphire crystal with a doping concentration of 0.05 wt. %. To achieve low-loss operation across a wide tuning range, the crystal was cut at Brewster's angle of 60.4°. The nonlinear medium was a $3 \times 3 \times 50$ mm^3 type-I noncritical phase-matched ($\theta = 90°$, $\varphi = 0°$) LBO crystal. It was coated with anti-reflection (AR) films at 532 nm, 920–1000 nm, and 1100–1200 nm, and mounted on a precision rotation stage to enable rotation about the beam propagation axis. The rotation angle α was defined as the angle between the polarization of the intracavity laser field and the crystallographic xOy plane of the LBO crystal. A birefringent filter composed of two quartz plates (0.5 mm and 2 mm thick, respectively) was placed at Brewster's angle for wavelength tuning and preliminary linewidth narrowing. Two uncoated etalons (0.5 mm and 10 mm thick, respectively) were used for further linewidth compression. The output coupler was a broadband polarizing beam splitter (PBS) with an extinction ratio exceeding 1000:1 in the 960–1000 nm band. The round-trip passive loss is estimated to be approximately 3.2% and has been incorporated into the theoretical simulation and experimental design. Two independent 532 nm ns pulsed lasers served as the pump sources (Pump1 and Pump2) for the Ti:sapphire and LBO crystals, respectively. Both sources operated at a repetition rate of 4 kHz with a pulse width of 20 ns and delivered output powers of 12 W (Pump1) and 40 W (Pump2). A digital delay generator (DDG) was used to synchronize Pump2 with the intracavity Ti:sapphire laser pulse, which enabled precise control of their temporal overlap. In order to achieve the efficient conversion, the waist radius of the laser beam of Pump1 was shaped to 322 μm via an optical coupling system OCS_1 to pump the Ti:sapphire crystal. The threshold pump power for the Ti:sapphire laser was measured to be 9.5 W. When Pump1 was increased to 12 W, the laser reached a state of stable operation with a narrow linewidth. All cavity mirrors were coated with high-reflection (HR) films, which ensured that the vast majority of the generated laser beam resonated within the cavity. Subsequently, the laser beam of Pump2 was introduced to pump the LBO crystal. The waist radius of Pump2 was optimized to 268 μm via OCS_2 and the temperature of LBO crystal was finely tuned to adjust the parametric signal wavelength to that of the Ti:sapphire laser. At the same time, the relative injection delay between two pump pulses was precisely optimized using a digital delay generator (DDG). The output powers versus the crystal rotation angle α for Pump2 powers of 10 W, 20 W, 30 W, and 40 W were firstly measured and the results were shown in Fig. 4(a). When the operating wavelength was set to 992 nm and the pump power increased, the optimal output angle progressively shifted towards larger values. At a pump power of 40 W, the maximum output power of 9.2 W was achieved at $\alpha = 60.5°$ and thus validated the model's reliability.

Due to the non-ideal reflectivity of mirror M_2, a portion of the intracavity light leaked through it. To characterize the unidirectional operation of the hybrid cavity, we simultaneously measured the power of both forward (CCW) and backward (CW) propagating light leaking from M_2. When only the Ti:sapphire laser worked, the forward and backward powers were both approximately 9 mW. As shown in curve (i) of Fig. 4(b), with the introduction and subsequent increase of Pump2 power, the OPO reached threshold and began to suppress the backward oscillation. Once Pump2 power exceeded 4 W, the backward power continued to drop. When Pump2 power exceeded 24 W, the backward power was suppressed to as low as 0.5 mW, a residual

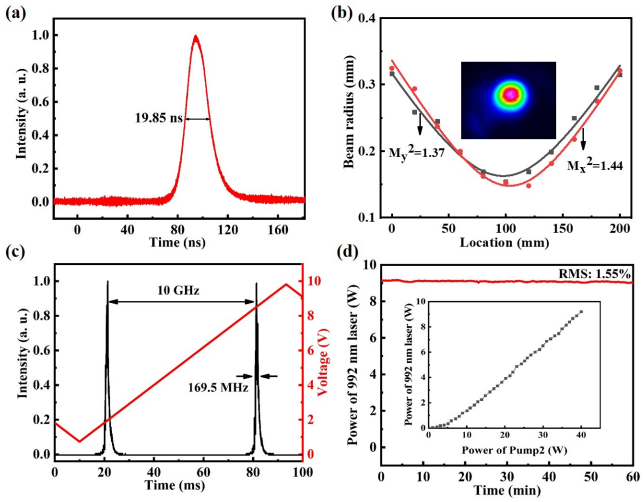


Fig. 5. Laser characteristics of the hybrid cavity output at 992 nm. (a) Pulse profile. (b) Beam quality M^2 factor measurement. (c) Linewidth measurement based on Fabry–Perot scanning. (d) Output power curve and power stability.

level that was mainly attributed to the early-stage oscillation of the Ti:sapphire laser before the OPO was fully established. As shown in curve (ii) of Fig. 4(b), because the forward (CCW) beam contains both Ti:sapphire and parametrically generated light, its power rose quickly once Pump2 power was exceeded 4 W, and the growth rate moderating slightly when Pump2 power exceeded 24 W. The strong contrast between forward and backward optical powers confirmed that the hybrid cavity achieved self-isolation through its intrinsic non-reciprocal gain mechanism, as the forward parametric gain depleted the shared Ti:sapphire upper-level population and diverted the gain originally available for the backward direction into the forward beam. This self-isolation not only enabled stable unidirectional operation without an external optical isolator but also significantly improved the output stability of the laser system.

The key output laser parameters under these conditions were summarized as follows. The pulse width measured with a photodetector (EOT ET-3500) and an oscilloscope (Tektronix DPO7254) was 19.85 ns as shown in Fig. 5(a). The beam quality factors were $M_x^2 = 1.44$ and $M_y^2 = 1.37$ measured by a beam quality analyzer (M2MS-BC207VIS/M, Thorlabs) and as presented in Fig. 5(b). A narrow linewidth of 169.5 MHz obtained via a scanning Fabry–Perot interferometer (SA210-8B, Thorlabs) is displayed in Fig. 5(c). Figure 5(d) shows both the output power versus Pump2 power and the long-term power stability. Specifically, at 992 nm with Pump2 at 40 W, the output power reached 9.2 W, and its stability over 1 hour of continuous recording showed an RMS value of 1.55%, as measured with a power meter (Ophir 30 A-BB-18 sensor).

Benefiting from the broadband AR/HR coatings on all intracavity optics, the hybrid cavity laser achieved broad wavelength tunability. By rotating the BRF and simultaneously adjusting the temperature of the LBO nonlinear crystal from 144.27°C to 147.43°C, the laser wavelength was continuously tuned from 963.26 nm to 1003.32 nm and a tuning range of 40.06 nm was achieved, as shown in Fig. 6.

In summary, we demonstrated a novel hybrid laser cavity based on the polarization-controlled integration of a Ti:sapphire gain medium with an intracavity OPO. By rotating the LBO

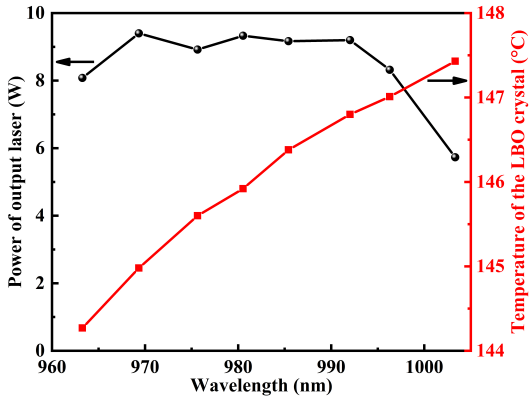


Fig. 6. Tuning characteristic of the output laser.

crystal and utilizing a polarizing beam splitter, we achieved the independent control over the low-loss oscillation of the *p*-polarized Ti:sapphire seed and efficient extraction of the *s*-polarized parametric signal. This approach resolved the conflict in output-coupling requirements between the two gain mechanisms. The laser generated 9.2 W of average power with a narrow linewidth of 169.5 MHz at 992 nm, which corresponded to an optical-to-optical efficiency of 17.7%. Moreover, the output wavelength was tuned from 963.26 nm to 1003.32 nm with a maximal tuning range of 40.06 nm. Through dynamic impedance matching and built-in nonreciprocal gain, this design ensured unidirectional operation without an optical isolator, which resulted in a compact, stable source that provided a practical solution for high-performance tunable near-infrared lasers.

Funding. National Natural Science Foundation of China (62575163, 62405170); National Key Research and Development Program of China (2022YFC2204003); Funding from the National Key Laboratory of Particle Transport and Separation Technology (KWKF-2024-2).

Disclosures. The authors declare no conflicts of interest.

Data availability. Data underlying the results presented in this paper are not publicly available at this time but may be obtained from the authors upon reasonable request.

REFERENCES

1. X. Zhou, Y. Xia, J. Uchitel, *et al.*, Biomed. Opt. Express **14**, 3234 (2023).
2. T. Heindel, J.-H. Kim, N. Gregersen, *et al.*, Adv. Opt. Photon. **15**, 613 (2023).
3. Z. Xu, Y. Wu, L. Tian, *et al.*, Phys. Rev. Lett. **111**, 240503 (2013).
4. X. Jia, Z. Yan, Z. Duan, *et al.*, Phys. Rev. Lett. **109**, 253604 (2012).
5. S. Yang and Y. Shen, Appl. Opt. **64**, 603 (2025).
6. H. Xuan, C. Qu, S. Ito, *et al.*, Opt. Lett. **42**, 3133 (2017).
7. H. Turcicova, O. Novak, L. Roskot, *et al.*, Opt. Express **27**, 24286 (2019).
8. G. T. Maker and A. I. Ferguson, Opt. Lett. **15**, 375 (1990).
9. T. Walther, M. P. Larsen, and E. S. Fry, Appl. Opt. **40**, 3046 (2001).
10. X. Ding, Y. Zou, L. Zou, *et al.*, Chin. Opt. Lett. **4**, 96 (2006).
11. Y. Bai, X. Ding, X. Dai, *et al.*, Opt. Laser Technol. **163**, 109401 (2023).
12. X. Fang, C. Cui, K. Zhang, *et al.*, Opt. Express **33**, 8632 (2025).
13. L. Hui-Qing, G. Ai-Cong, B. Yong, *et al.*, Chin. Phys. Lett. **22**, 1694 (2005).
14. J. Qin, J. Song, X. Cao, *et al.*, Opt. Lett. **48**, 4973 (2023).
15. X. Cao, Y. Chen, F. Duan, *et al.*, Opt. Lett. **50**, 4374 (2025).
16. R. L. Sutherland, in *Handbook of Nonlinear Optics*, 2nd ed. (CRC Press, 2003), Chap. 3, p. 142.